Iron Slag Permeable Reactive Barrier for PFOA Removal by The Electrokinetic Process

Namuun Ganbat[1], Faris M. Hamdi[1], Ibrar Ibrar[1], Ali Altaee*[1], Lilyan Alsaka[1], Akshaya K. Samal[2], John Zhou[1], Alaa H. Hawari[3]

[1]Centre for Green Technology, School of Civil and Environmental Engineering, University of Technology Sydney

[2]Centre for Nano and Material Sciences, Jain University, Ramanagara, Bangalore 562 112, Karnataka, India

[3]Department of Civil and Architectural Engineering, College of Engineering, Qatar University, PO Box 2713, Doha, Qatar

Corresponding Author: Ali Altaee, Email: ali.altaee@uts.edu.au

Graphical Abstract

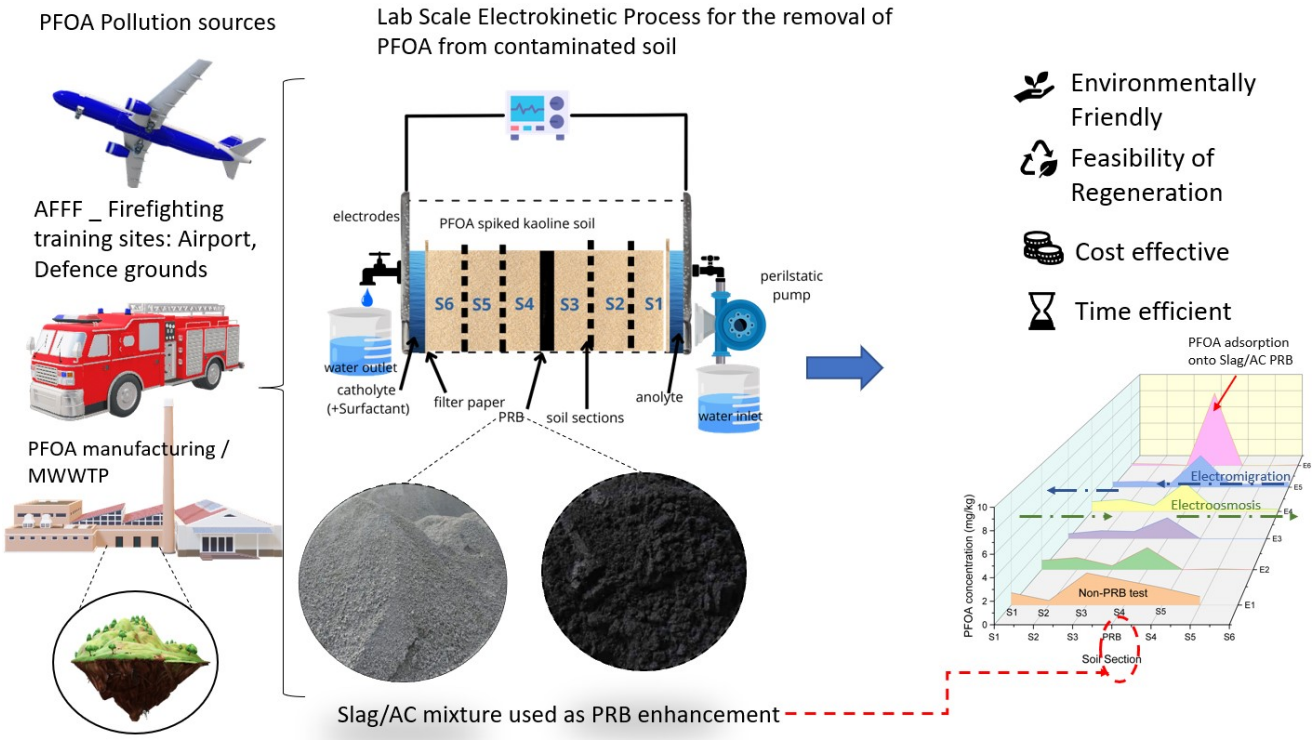

Abstract

The efficacy of the Standalone Electrokinetic (EK) process in soil PFAS removal is negligible, primarily due to the intersecting mechanisms of electromigration and electroosmosis transportation. Consequently, the redistribution of PFAS across the soil matrix occurs, hampering effective remediation efforts. Permeable reactive barrier (PRB) has been used to capture contaminants and extract them at the end of the EK process. This study conducted laboratory-scale tests to evaluate the feasibility of the iron slag PRB enhanced-EK process in conjunction with Sodium Cholate (NaC) biosurfactant as a cost-effective and sustainable method for removing PFOA from the soil. A 2 cm iron slag-based PRB with a pH of 9.5, obtained from the steel-making industry, was strategically embedded in the middle of the EK reactors to capture PFOA within the soil. The main component of the slag, iron oxide, exhibited significant adsorption capacity for PFOA contamination. The laboratory-scale tests were conducted over two weeks, revealing a PFOA removal rate of more than 79% in the slag/activated carbon PRB-EK test with NaC enhancement and 70% PFOA removal in the slag/activated carbon PRB-EK without NaC. By extending the duration of the slag/AC PRB-EK test with NaC enhancement to three weeks, the PFOA removal rate increased to 94.09%, with the slag/AC PRB capturing over 87% of the initial PFOA concentration of 10 mg/L. The specific energy required for soil decontamination by the EK process was determined to be 0.15 kWh/kg. The outcomes of this study confirm the feasibility of utilizing iron slag waste in the EK process to capture PFOA contaminants, offering a sustainable approach to soil decontamination. Combining iron slag PRB and NaC biosurfactant provides a cost-effective and environmentally friendly method for efficient PFOA removal from soil.

***Keywords**: Electrokinetic, Soil remediation, PFAS treatment, Permeable reactive barrier, Enhanced Electrokinetic*

Introduction

Perfluoroalkyl substances (PFAS) are an anthropogenic environmental pollutant that has attracted public attention as an emerging organic contamination of concern due to their potential adverse health effects and persistent, non-biodegradable accumulation in the environment, humans and wildlife. Perfluorooctanoic acid (PFOA) is one of the most prevalent PFAS chemicals detected in the environment [1]. PFOA possesses a hydrophobic fluorinated alkyl chain, contributing to its thermal and chemical stability. Additionally, PFOA features a polar functional group at the end, enabling its solubility and affinity for transport in the environment. Consequently, PFOA can migrate long distances through soil and water, potentially contaminating drinking water supplies [2]. The presence of perfluorooctanoic acid (PFOA) originating from aqueous film-forming foam (AFFF) is a matter of substantial concern, particularly in regions characterized by extensive AFFF utilization, such as airports and military bases. These locations often serve as firefighting training grounds, thereby intensifying the potential for PFOA contamination [3]. Using PFOA containing AFFF for fire suppression releases PFOA and other PFAS into the environment, contaminating soils and groundwater. Also, reports indicate that PFOA is released into the environment during production due to its extensive use in industrial and consumer goods [4]. In addition, the introduction of PFOA into the soil can occur through various pathways. This includes the disposal of PFOA-containing products in landfills and the transportation of PFOA through the air, which can subsequently be deposited onto soil via atmospheric deposition. Moreover, the release of PFOA-containing aerosols from industrial processes or the burning of materials containing PFOA can also contribute to the presence of PFOA in soil [5]. Due to their properties, PFOA can persist in the environment for a long time and migrate significant distances from the source of contamination [6]. PFOA is particularly resistant to biodegradability, vaporization and highly bioaccumulative; hence, some plants may absorb them from soil or water. In that situation, it enters the food chain posing a significant health risk to humans and wildlife. Most residents of industrialized nations will have some PFAS in their systems because of their widespread use [7]. Exposure to PFOA has been linked to several health effects, including liver damage, immune

system dysfunction, and an increased risk of cancer. However, long-term health has yet to be extensively studied [8]. As a result, efforts are being made to reduce the PFOA and other PFAS-containing products and remediate contaminated areas.

Several review articles have summarised recent technologies and remediation techniques for removing PFAS [4, 9, 10]. Immobilization methods such as stabilization and solidification have been utilized frequently to stop the migration of PFAS from entering the groundwater, surface water and surrounding environment [1, 11, 12]. Extensive research has been conducted on utilizing granular activated carbon (GAC) and biochar as potential methods for immobilizing PFAS within the soil matrix. In a pilot study to determine the viability of stabilization and solidification treatment, 6 tonnes of AFFF-contaminated soil were used, resulting in an average removal rate of 92% for PFOA and PFOS. However, the long-term stability assessment is a limitation of solidification and stabilization treatment [13]. Thermal treatment has been used widely to remove PFAS from contaminated soil [14]. When implementing thermal heating techniques, excavating contaminated soil becomes necessary, posing inherent risks to human health during the digging and transportation phases. Alternatively, subjecting contaminated soil to high-temperature thermal treatment proves inefficient, environmentally damaging, and expensive, resulting in industrial waste generation [9]. Mechanochemical treatment has shown significant promise in reducing the levels of PFOA and PFOS in dry sand, achieving impressive removal rates of 99% and 98%, respectively, in AFFF-contaminated soil [15]. A soil-washing plant employing physical and chemical processes has been employed for remediation. These processes involve fractionating soil particles based on size and extracting PFASs into the aqueous phase, followed by treatment of the contaminated water using granular activated carbon and ion exchange resins. This comprehensive approach has resulted in average removal efficiencies of 97.1% for PFOA and 94.9% for PFOS [16]. However, a notable drawback is associated with excavating and transporting contaminated soil to treatment facilities, which can be costly. As a result, an in-situ soil washing method was investigated and compared to an excavated soil washing technique, yielding a removal efficiency of 76% for the in-situ method. [17]. The bioremediation of PFAS has been the

subject of several studies. However, due to the limited understanding of the degradation mechanisms involved, the definitive degradation pathway for PFAS remains unclear. Nevertheless, bioremediation shows promising potential as an in-situ remediation process for PFAS contamination [18, 19]. The feasibility of various lab-scale electrochemical treatments for removing PFAS has been evaluated, demonstrating that PFAS exhibits mobility within the EK process when subjected to an electric field. However, electrokinetic treatment alone was insufficient to eliminate PFAS. Consequently, the incorporation of enhancing agents into the EK process has been investigated to improve the removal efficiency of PFAS contaminants [20-22].

Electrokinetic remediation involves the mobilization of contaminants by applying a direct electric current, where charged contaminants are transported towards the cathode or anode via electromigration and electroosmosis phenomena [23]. Various approaches have been employed to enhance the efficiency of electrokinetic remediation, including surfactants and PRBs, resulting in improved removal of heavy metals and organic contaminants [24, 25]. Researchers have recently focused on environmentally sustainable methods to enhance electrokinetic processes. PRB-enhanced electrokinetic studies have demonstrated successful remediation outcomes in numerous lab-scale experiments, particularly when utilizing agricultural or industrial waste as PRB media, offering practicality and sustainability through waste material reuse [26]. In recent years, the combination of PRBs and electrokinetic processes has gained significant attention due to their environmental compatibility, versatility, scalability, and cost-effectiveness. This approach has proven effective in increasing contaminant removal efficiency, especially in low-permeability soils [27]. PRB-enhanced EK tests have demonstrated successful implementation in soils contaminated with organic pollutants. Zero valent iron/Activated carbon enhanced EK process coupled with biosurfactant for the removal of persistent organic pollutants, achieved a removal rate of 64.6% [28]. Besides, carbonized food waste has been employed in the EK process to extract copper with an average removal efficiency of 53.4%-84.6% [29]. Compost was applied as PRB in the EK process to extract copper in a lab-scale study. The experimental results were 84.09% removal, and after two cycles of regeneration and reuse, the

118 removal efficiency was 74.11% [30]. PRBs offer several advantages in the EK process, including the in-
119 situ adsorption, degradation, or immobilization of contaminants, without bringing them to the surface
120 [31]. While surfactant-enhanced EK tests have shown the potential to remove contaminants from
121 specific regions, the remaining pollutants often accumulate in the soil. In contrast, PRB-enhanced
122 processes can effectively address these challenges and overcome these limitations [32]. Research has
123 reported that coupling various types of PRB with EK can significantly improve removal efficiency [30,
124 32-34]. Incorporating PRBs within the soil chamber has proven effective in adsorbing, degrading, or
125 precipitating contaminants transported through electroosmosis or electromigration processes.
126 Among the various materials used for PRBs, activated carbon (AC) stands out as a cost-effective option
127 due to its large surface area and exceptional adsorption capacity for organic contaminants and heavy
128 metal ions. Accordingly, AC is frequently included in PRBs for EK processes. When selecting a suitable
129 PRB, it is crucial to consider factors such as cost efficiency and environmental sustainability. In this
130 regard, researchers have explored the use of granular activated carbon (GAC), biochar, and compost
131 as environmentally sustainable approaches to enhance the EK process [30, 35]

132 Steel-making slag is a residual waste material generated during steel production, serving as a by-
133 product of the industry [36, 37]. Due to its unique surface properties, slag has been employed as a
134 stabilization and solidification method in soil and wastewater remediation [36]. The novelty of this
135 research proposes using an environmentally sustainable approach for soil remediation by employing
136 an iron slag/activated carbon mixture as a PRB, thereby enhancing the efficiency of the EK process for
137 removing PFOA contamination [18, 19]. In light of this information, the iron slag/AC PRB will be
138 introduced at the soil middle section to capture the PFOA contaminant. To our knowledge, steel slag-
139 PRB has not been used for PFOA removal from contaminated soils by the EK process. Previous studies
140 revealed that the interaction between electromigration and electroosmosis transportation
141 mechanisms leads to the accumulation of PFOA contaminants, specifically in the middle section of the
142 soil within the reactor cell at the end of the EK process. The main slag component is iron oxide, which
143 has a high adsorption capacity for anionic compounds. The affinity of PFOA adsorption into iron oxide-

144 based PRB will enhance its removal from the soil at the end of the EK process. The study also evaluated
145 the impact of using different percentages of iron slag/activated carbon (AC) mixture PRB and process
146 duration on PFOA removal by the EK process.

147 **Materials and Method**

148 **2.1 Materials, soil preparation, and analysis.**

149 For the electrokinetic (EK) experiments, a kaolin clay sample obtained from Keane Ceramic Pty
150 Australia was chosen as the model soil. This selection was based on its characteristics: low
151 permeability, low carbon content, and low cation exchange capacity. The supplier provided detailed
152 information about the properties of the kaolin soil used in the EK tests, summarized in Table 1. The
153 absence of organic matter and the non-reactivity of the kaolin soil make it ideal for studying the
154 mobility of PFOA under direct electric fields in the EK system without any interference.

155 The kaolin soil was artificially spiked with PFOA at 10 mg/kg for all EK experiments to simulate the
156 contaminated soil conditions. According to Mahinroosta and co-workers, the maximum PFOA
157 concentrations detected in Australia in contaminated sites varied from 10 mg/kg to 460 mg/kg [9].
158 Each EK experiment involved 1000 g of kaolin soil. Initially, 1 g of PFOA was completely dissolved in
159 1000 mL of Milli-Q water to create a 1000 ppm stock solution. This stock solution was further diluted
160 to 10 mg/L for each experiment. The prepared 1 L solution was thoroughly mixed with 1000 g of kaolin
161 soil. The spiked soil was then kept at room temperature for at least 72 hours, with periodic stirring to
162 ensure a consistent distribution of PFOA throughout the soil matrix. The saturated soil was loaded into
163 the reactor in layers and compacted uniformly to ensure an even distribution of PFOA.

164 For the PRB, iron slag was mixed with AC purchased from Sigma-Aldrich (Australia) and was employed
165 in the EK experiments. Steel-making slag was obtained from the Environmental Engineering
166 Laboratory, University of Technology Sydney. The iron slag-activated carbon (AC) PRB was placed in
167 the soil middle section where most PFOA accumulates [21]. At the end of the EK process, the PRB will
168 be removed from the soil for PFOA extraction, benefiting from the PRB high-permeability, which will

be more economical and faster than the fine-grained low-permeability kaolinite soils. A multimeter (Thermo Scientific model EUTECH PC 450) was used to measure the soil's pH and electrical conductivity by making slurries with a dry soil-to-water ratio of 1:5 (w:v) [40]. The PFOA concentration in the soil was analyzed using liquid chromatography-mass spectrometry (LC-MS) (LC/MS 8060, Shimadzu, shim pack column 1.6 m, 2.0 mm 50 mm) as the analytical instrument before and after the EK tests. Morphological and chemical characteristics of PRBs were determined using Energy Dispersive X-ray spectroscopy (EDX) in conjunction with Scanning Electron Microscopy (SEM) by Zeiss Evo-SEM with an acceleration voltage of 15 kV for EDS collection, a chemical microanalysis technique. Fourier Transform Infrared Spectroscopy (FTIR) (Miracle-10; Shimadzu) was used to analyze the surface functional groups of PRBs before and after EK tests. The specific surface area of PRBs before and after EK treatment was determined using Brunauer-Emmett-Teller (BET) nitrogen adsorption-desorption isotherms and the Barrett-Joyner-Halenda (BJH) method, respectively, by using a Micrometrics 3-FlexTM surface characterization analyzer at 77K.

Table 1: Physicochemical properties of kaolin soil and PRB

Parameters	Soil	Slag/AC
Particle size analysis (%)	46.81	2.47
Clay (%)	51.17	NA
Sand/Silt (%)	2.02	NA
Permeability (m/s)	4×10^{-10}	2.54×10^{-2}
Density (g/cm^3)	1.45	1.53
Porosity (kg/m^3)	633	-
Organic matter	Negligible	NA
TDS (mg/L)	145	NA
pH	5.24 ± 0.03	9.51
Electrical conductivity (mS/cm)	0.46	0.96

2.2 Electrokinetic cell setup and test design.

Fig. 1 displayed the schematic setup diagram of the EK tests, consisting of a 23 x 8 x 11 cm^3 plexiglass reactor. The reactor comprises two electrode compartments at either end: a soil compartment, a PRB compartment, and an electrolyte reservoir. In the middle of the soil compartment, 2 cm PRB sandwiched between two filter papers was employed, and contaminated soil was loaded onto both

sides. Filter paper (5-13 µm LLG) Labware supported by a perforated plexiglass plate was placed between the electrode chamber and the soil compartment to prevent soil from entering the electrolyte chambers. A constant current was applied using a DC bench power supply (EA-PS 3016-10B, EA Electro-Automatik). The electric current and voltage were measured and recorded hourly using a multimeter (Keithley 175 Autoranging multimeter). The electrode chambers on either side of the reactor were equipped with two (15 x 1 cm) graphite rod electrodes (Graphite Australia Pty Ltd). Based on the previous study results, the biosurfactant sodium cholate (NaC) was added to the catholyte solution (Sigma-Aldrich). NaC outperformed conventional surfactants in enhancing PFOA removal in the EK process [21]. Regular injections of ultra-pure water were made into the anolyte compartment to compensate for water loss brought on by electroosmotic flow. Throughout the experiment, electroosmotic flow and current intensity were periodically measured.

The EK experiments were conducted at room temperature without pH control with an initial steady current of 20 mA. **Table 3** provides details on the six EK experiments. The anolyte was MQ water, and the catholyte was a 5% (w/w) NaC biosurfactant. The fluid level in the inflow reservoir was maintained at a constant level to maintain a continuous hydraulic gradient throughout the soil. The EK test was carried out for two weeks using PFOA-contaminated kaolin soil with an initial 10 mg/kg concentration.

To evaluate the effectiveness of the PRB-enhanced EK test, E1 was conducted as a reference experiment to examine the removal of PFOA without a PRB with but only 5% w/w NaC biosurfactant introduced at the cathode. Experiment E2 reviewed the efficacy of slag/AC-PRB coupled with NaC biosurfactant, whereas experiment E3 investigated the effects of higher slag proportion, slag/AC-PRB coupled with a biosurfactant. Experiment E4 studied the performance of regenerated slag/AC-PRB EK coupled with biosurfactant. Experiment E5 studied the performance of slag/AC-PRB EK treatment without biosurfactant. Lastly, experiment E6 examined the effects of the slag/AC-PRB EK test coupled with biosurfactant for 3 weeks. PRB was positioned in the middle of the reactor cell in all EK tests.

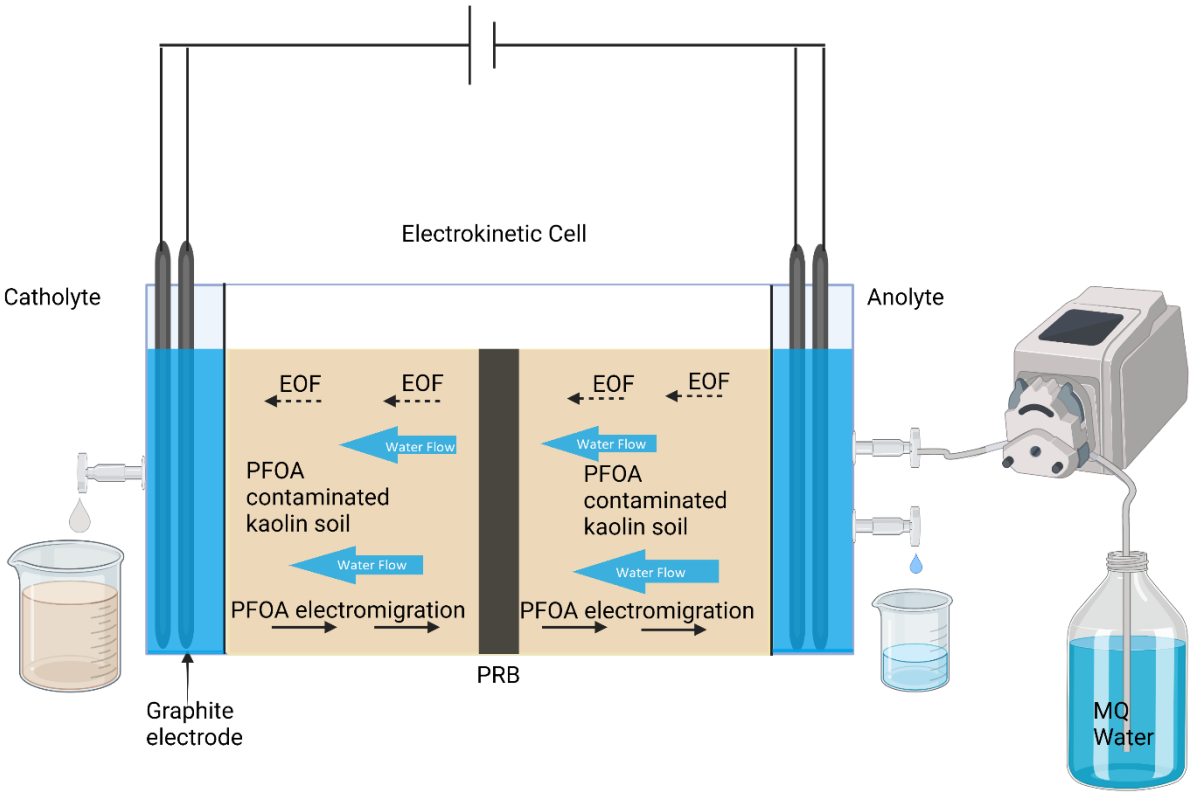

Figure 1: Schematic diagram of the electrokinetic cell setup

Table 2: Test design of bio-Surfactant enhanced EK tests coupled with Slag/AC PRB.

Exp No.	Target Contamination	Concentration of PFOA (mg/kg)	Surfactant and dosing point	PRB type and position	Surfactant Concentration (% w/w) Catholyte	Duration (days)
E1	PFOA	10	NaC/cathode	NA	5	14
E2	PFOA	10	NaC/cathode	Slag/AC (50/50) in the middle	5	14
E3	PFOA	10	NaC/cathode	Slag/AC (70/30) in the middle	5	14
E4	PFOA	10	NaC/cathode	Regenerated Slag/AC (70/30) in the middle	5	14
E5	PFOA	10	NA	Slag/AC (70/30) in the middle	NA	14
E6	PFOA	10	NaC/cathode	Slag/AC (70/30) in the middle	5	21

221 **2.3 PFOA analysis.**

222 The power supply was disconnected, and the test setup was disassembled after fourteen days
223 (experiments E1-E5) and twenty-one days (experiment E6). At the end of each test, aqueous solutions
224 from the anode and cathode chambers were collected, and the PFOA concentration, pH, and EC were
225 determined. The soil sample was divided into six equal sections, S1 to S6, from the anode to the
226 cathode. Duplicate samples were obtained from each section, and the soil pore water was separated
227 using a centrifuge (Beckman Coulter, Allegra Centrifuge V-15R). The remaining soil sample was dried
228 for 12 hours in a 105°C oven. The methods used in the previous study were used to extract PFOA from
229 a soil sample [21]. PFOA was extracted from each sample using triple methyl alcohol extraction, and
230 the extraction recovery for PFOA was around 92%. 5mL of methyl alcohol was added to 5g of dry soil,
231 shaken at 250 rpm for 60 minutes at 25^0C, sonicated for 30 minutes at 30^0C, and centrifuged for 10
232 minutes at 9000 rpm [41]. The supernatants were collected, diluted, and filtered (using a PTFE syringe
233 filter) before being transferred into vials for LC-MS/MS analysis (LC/MS 8060, Shimadzu, shim pack
234 column 1.6 m, 2.0 mm 50 mm). PRB was extracted in the same manner as soil samples. The removal
235 efficacy was calculated using the following equation:

236 $$\text{Removal efficiency } (\%) = \frac{C_0 - C_f}{C_0} \times 100 \qquad (1)$$

237 Equation 1, where C_0 and C_f are PFOA (mg/kg) concentrations initially and after EK treatment in the
238 soil sections (S1-S6 and PRB). A 1:5 (w/v) ratio of dry mass to DI water slurry was prepared to measure
239 the pH and EC of the soil and the PRB.

240 **3. Results and Discussion**

241 **3.1 Electric current**

242 The electric current mobilizes ionic species in the contaminated soil during the EK process. Water
243 electrolysis reaction generates hydronium ions at the anode and hydroxide ions at the cathode
244 electrode. The developed acid and alkaline front will migrate to the respective electrode in the soil.

Charged molecules will be solubilized as the acid front advances in the soil and migrate to respective cathodes. **Figure 2** depicts the change in electric current and voltage in the soil during different EK experiments. In general, the electric current was directly correlated with the electric charge level passing through the soil pores, with the inverse direction of the electrons' movement [42]. The electric current was about 20 mA at the beginning of the EK experiment and progressively declined over time [26, 42]. Because of the electrolysis reaction at the anode and increasing dissolved ions in the pore solution, the electric current initially remained constant at 20 mA for several hours. Since the electric current through the soil cell is strongly correlated with the concentration of free ions, the electric current is a significant factor influencing the utilization of contamination transport through the soil. The water electrolysis reaction and the migration of charged molecules to the opposite charge electrode can explain this phenomenon. The current decreased after 48 to 240 hours due to reduced soil conductivity caused by acid and alkaline front meeting and charged molecules accumulation in the soil specimen (**Figure 2a**). Contaminants are transported towards the electrolytic chambers and removed during the EK process. As a result, the electric current drops due to fewer charged particles in the soil. The gradual decline in the electric current could also be due to the electrodes' fouling caused by soil particles accumulation, reducing the electrode surface area.

As illustrated in **Figure 2a**, experiments E1 to E3 exhibited a constant current that slowly dropped over time. However, in experiment E1, the current dropped rapidly after 48 hours, probably due to the faster-increased soil resistivity as PFOA was accumulated in the soil sections. As stated previously, the rapid drop in current could be related to the depolarization effect associated with the acid and alkaline front due to water electrolysis at the anode and cathode, leading to soil pore clogging [23]. In experiments E2 and E3, the current remained at around 20 mA for almost 96 hrs, then fluctuated until dropping to a constant value at the end of the experiment. In experiment E3, the electric current fluctuated more than in experiment E2 before it stabilized and decreased after 216 hours. A Comparison of the electric current indicates that tests with a slag PRB recorded higher currents than tests without a slag PRB (experiment E1). The slight increase in the current can explain this due to the

high conductivity of the slag PRB. This observation agrees with previous studies where experiments conducted with a PRB recorded a higher electric current [32, 43]. The ionic species were transported to the opposite charge electrolytic chambers over time, decreasing the soil's ionic conductivity and resulting in a sharp current drop. During experiments E4 and E5, the electric current maintained stable at around 20 mA for 336 and 240 hours, respectively. Experiment E5 was conducted without the NaC enhancement agent, which probably affected the transport of ionic species and accumulation in the soil, leading to an increased soil resistivity. The longer constant current in experiments E4 and E5 can be explained by flushing fluid compensating for the loss of ionic species, reducing the soil resistance and increasing the current intensity [44]. The stable and constant current observed in experiment E4, where NaC was absent in the cathodic chamber, and experiment E5, where the slag PRB was regenerated, may be attributed to these factors. In these experiments, the migration of ions under the electric field occurred at a stable rate compared to other EK tests where fresh PRBs were used in combination with NaC. This stability can be attributed to the lower voltage values applied in experiments E4 and E5. The average current in experiment E4 was 19.75 mA and was 19.27 mA in experiment E5. Whereas in experiment E2, the average current was 10.51 mA, in experiment E3 was 13.39, and in experiment E6, it was 14.05 mA. However, the average voltage was higher in these tests. Experiment E6 was conducted for 3 weeks, and the current remained constant at 20 mA for 144 hours and gradually decreased, reaching 7 mA at the end of the experiment. Experiment E6 exhibited a steady decrease in the electric current over time. The reason could be PFOA accumulating in the PRB and less migration in the soil. Hence, there are fewer mobilized species in the soil for transportation. As the PFOA accumulated in the PRB, the ions gradually depleted, reducing the soil conductivity and causing a decrease in the current. The sorption onto PRB may have induced a slow diffusion of PFOA in the EK cell.

As depicted in **Figure 2**, the change in electric current is inversely proportional to the change in voltage. When the current is stable at around 20 mA, the voltage remains low, but as soon as the current starts to decrease, the voltage increases. Generally, the voltage of PRB-enhanced EK tests was

297 more stable than without a PRB. **Figure 2b** depicts the change in voltage over time in the electrokinetic
298 experiments E1 to E6. Experiment E1 reached the maximum voltage rapidly after 48 hours, indicating
299 a sharp increase in soil resistivity. The greater voltage in experiment E3 than in experiment E2 reflected
300 the fluctuation in the electric current in experiment E3. The voltage in experiments E4 and E5
301 remained stable for longer and slowly climbed up after almost 7 days due to the increased soil
302 resistivity over time. The prolonged stable voltage could be because it was lower than the EK tests.
303 The voltage increase in experiment E6 after 240 hours was due to the drop in the electric current
304 (**Figure 2a**) due to the increased soil resistivity, causing a sharp increase in the voltage.

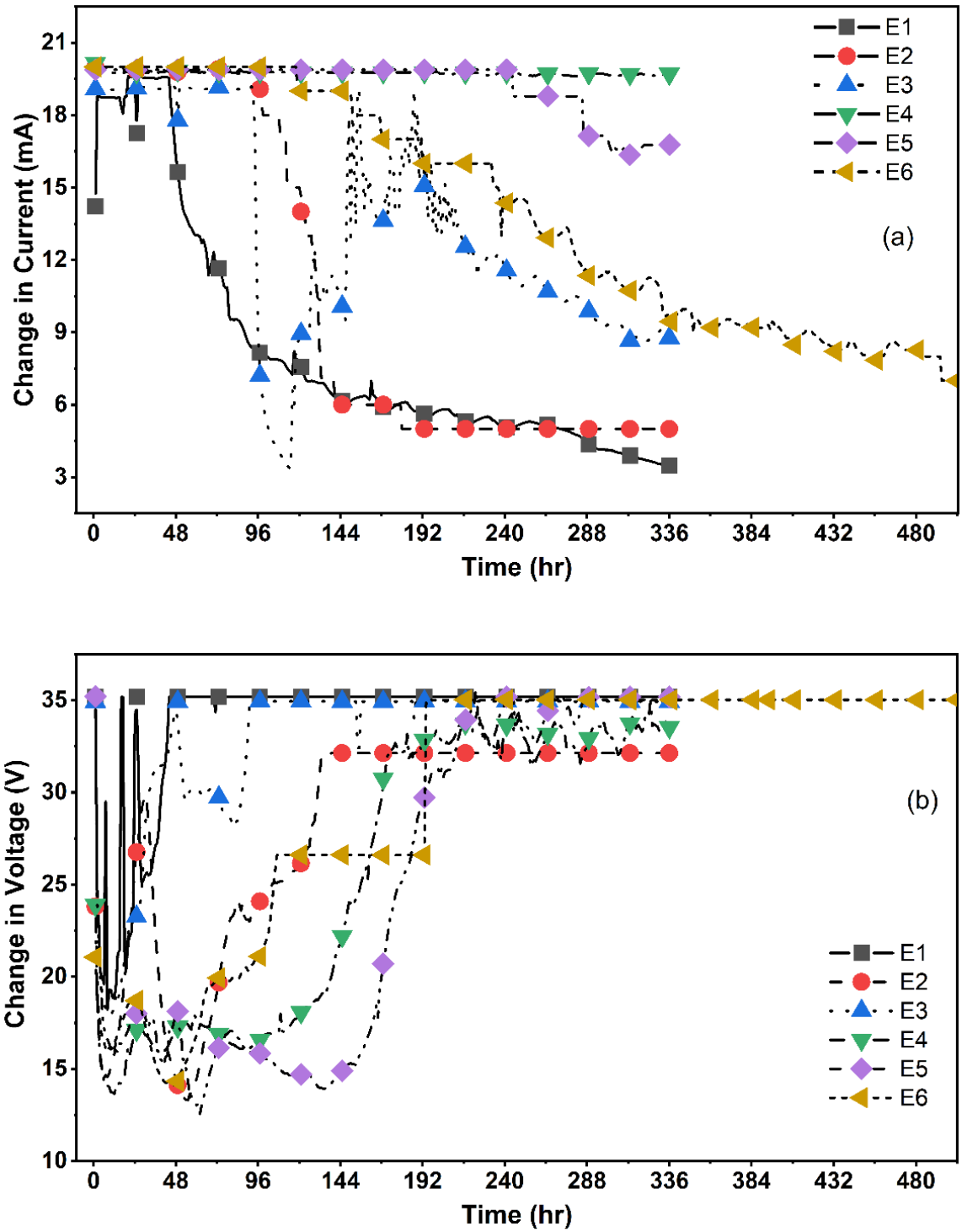

Figure 1: (a) Change in Current (mA) (b) Change in Voltage (V)

3.2 Soil pH and Electric conductivity

The pH distribution across the soil, ranging from the anode to the cathode (sections S1 to S6), following the completion of the EK experiments, is presented in **Figure 3a**. As shown in **Figure 3a**, the soil pH in sections near the anode region, sections (S1 to S3) exhibited an acidic nature, primarily attributed to

311 the rapid migration of the acid front caused by the electrolysis reaction, which generates H^+ ions. This
312 occurrence can be attributed to hydrogen ions' higher effective ionic mobility, approximately 1.8 times
313 faster than hydroxide ions. [23]. **Figure 3a** clearly depicts the pH variations in the soil sections for both
314 non-permeable reactive barrier-enhanced experiment E1 and PRB-enhanced experiments E2-E6. In
315 experiment E1, the pH levels in soil sections S1 to S4 remain consistently acidic (pH3 to pH3.9), with a
316 minor increase observed near the cathode, reaching pH4.8 in section S5, due to the faster migration
317 of H^+ ions compared to OH^- ions. In contrast, in PRB-enhanced experiments E2 and E3, a noticeable
318 increasing trend in pH is observed from the permeable reactive barrier towards soil sections S4 to S6.
319 This trend can be attributed to the initial pH of the PRB, which is approximately 9, and its influence on
320 the transportation of H+ ions across the soil sections near the cathode. Notably, the pH at the cathode
321 chamber remains around 12, while the pH values in the sections near the cathode (S4 to S6) fluctuate.
322 Specifically, in experiment E2, the pH ranges across soil sections S1 to S3 are 2.94-3.00, while the pH
323 ranges in sections S4 to S6 are 7.90-8.53. In experiment E3, the pH ranges across soil sections S1 to S3
324 are 2.54-2.92, while the pH ranges in sections S4 to S6 are 8.65-9.73. The pH values for the PRB in
325 experiments E2 and E3 are 8.37 and 9.54, respectively. The slight increase in pH for the PRB can be
326 attributed to a higher slag ratio within the PRB. In the regenerated PRB-enhanced (PRB-EK) test E4, a
327 similar pH trend across the soil sections is evident, as observed in experiments E2/E3. In contrast,
328 experiment E5 was conducted without using NaC biosurfactant, resulting in pH values ranging from
329 3.11 to 3.83 in sections S1 to S3 and from 9.81 to 10.26 in sections S4 to S5. The slight increase in pH
330 across the soil sections can be attributed to the absence of biosurfactants. Lastly, experiment E6 was
331 conducted over 3 weeks, revealing a pH range of 3.72-3.80 in sections S1-S3 and 5.34-7.47 in sections
332 S4-S6. Experiment E6 demonstrated the lowest pH range in sections S4-S6 due to the continuous
333 generation and transportation of H^+ ions across the soil sections over an extended period. The higher
334 ionic mobility of H^+ ions in the electrokinetic (EK) process could lead to their dominance and
335 subsequent lower pH values in sections S4-S6 compared to other experiments. The higher pH in
336 sections close to the cathode would impart a negative charge on the soil surface, decreasing PFOA

adsorption on the soil. As the soil acquires a negative charge, PFOA adsorption on the soil decreases due to reducing the electrostatic interaction with the negatively charged PFOA compound [45]. Previous studies observed that PFOA had higher adsorption affinity at acid soil pH [46]. The pH-dependent adsorption of PFOA agrees with earlier research where PFOS adsorption on kaolinite was studied, and experimental results observed decreased adsorption with an increase in pH [47].

Interestingly, in the E2 experiment, the soil pH in sections S1 to S3 was lower than the initial pH (pH 2.9 to 3), as shown in **Figure 3b**. It significantly increased in section S4, reaching pH 7.9 and gradually increased to pH 8.53 in section S6. As shown in **Figure 3c,** soil pH in sections S1 to S3 was 2.54 to 2.92 and significantly increased to 8.65 in soil section S4, and it continued to increase to section S6 with pH 9.73. The sudden increase in the soil pH in section S4 was probably attributed to the alkaline pH of the iron slag PRB (pH 9.5), which hindered the advancement of acid in the soil. Also, the advancement of OH^-ions from the cathode influenced the pH values in soil sections S4 to S6. In experiment E4, in sections S1 to S3, the recorded pH was pH3.02 to pH3.3 (**Figure 3d)** and drastically increased to 8.86 in soil section S4, then kept increasing to 9.35 in section S6 near the cathode. The higher pH in the cathode region for experiment E3 could be due to the higher slag content in the PRB. **Figure 3e** shows that the sections S1 to S3 pH were from pH3.11 to pH3.83 in experiment E5, and it increased significantly to pH 9.81 in the soil section S4. The highest soil pH in experiment E5 was pH10.26 in section S6, and it could be due to the absence of biosurfactants and the rapid advancement of OH^-in these soil sections. Experiment E6 also exhibited low pH3.72 to pH3.8 in sections S1 to S3 (Figure 3f) and increased to pH5.34 to pH 7.47 in sections S4 to S6. The increase in the soil pH from sections S3 to S4 was insignificant in experiment E6 due to the longer experimental time that allowed the acid to sweep across the soil specimen.

Soil conductivity, as seen in **Figure 3**, is inversely proportional to the pH of the soil. A Similar trend was observed in the previous studies conducted [22]. Previous studies agree with these results that soil EC is inversely related to soil pH [21, 30]. The soil's electric conductivity (EC) plays a vital role in the EK

362 treatment, which involves the movement of the contaminants and other charged particles under the
363 direct electric current. During the EK process, the transportation of charged particles to the anode and
364 cathode creates a concentration gradient that can result in soil resistivity and change in the soil pH.
365 The soil has a more remarkable ability to transmit electrical charges when the EC of the soil is high;
366 however, removing ionic species during the electrokinetic treatment can cause a decrease in electric
367 conductivity. **Figure 3** suggests that the electric conductivity is lower in soil regions with high PFOA
368 removal. The soil EC showed a progressive reduction from the anode to the cathode region in
369 experiments E1 to E6, indicating that more free ions are in the anode than in the cathode region. In
370 general, the EC is higher in sections S1 to S3 in all EK tests due to the concentration of the ionic species,
371 which is correlated with free protons. In all experiments, the EC decreased in the soil sections S4 to S6
372 due to the acid and alkaline fronts meeting near the cathode region. As shown in **Figures 3b and 3c,**
373 there was a significant difference in the PRB EC of experiments E2 and E3 depending on the ratio of
374 iron slag to AC in the PRB and the metal ions impurities captured by the PRB. For example, the PRB EC
375 was 28.1 µS/cm in experiment E2 and 850.3 µS/cm in experiment E3. Furthermore, the EC of recycled
376 PRB in experiment E4 (**Figure 3d)** was 79.3 µS/cm and 356.6 µS/cm in experiment E5 (**Figure 3e)**. The
377 highest EC in PRB was 3460 µS/cm after 3 weeks of testing in experiment E6 (**Figure 3f)** and could be
378 attributed to the longer experimental time and higher PFOA adsorption.

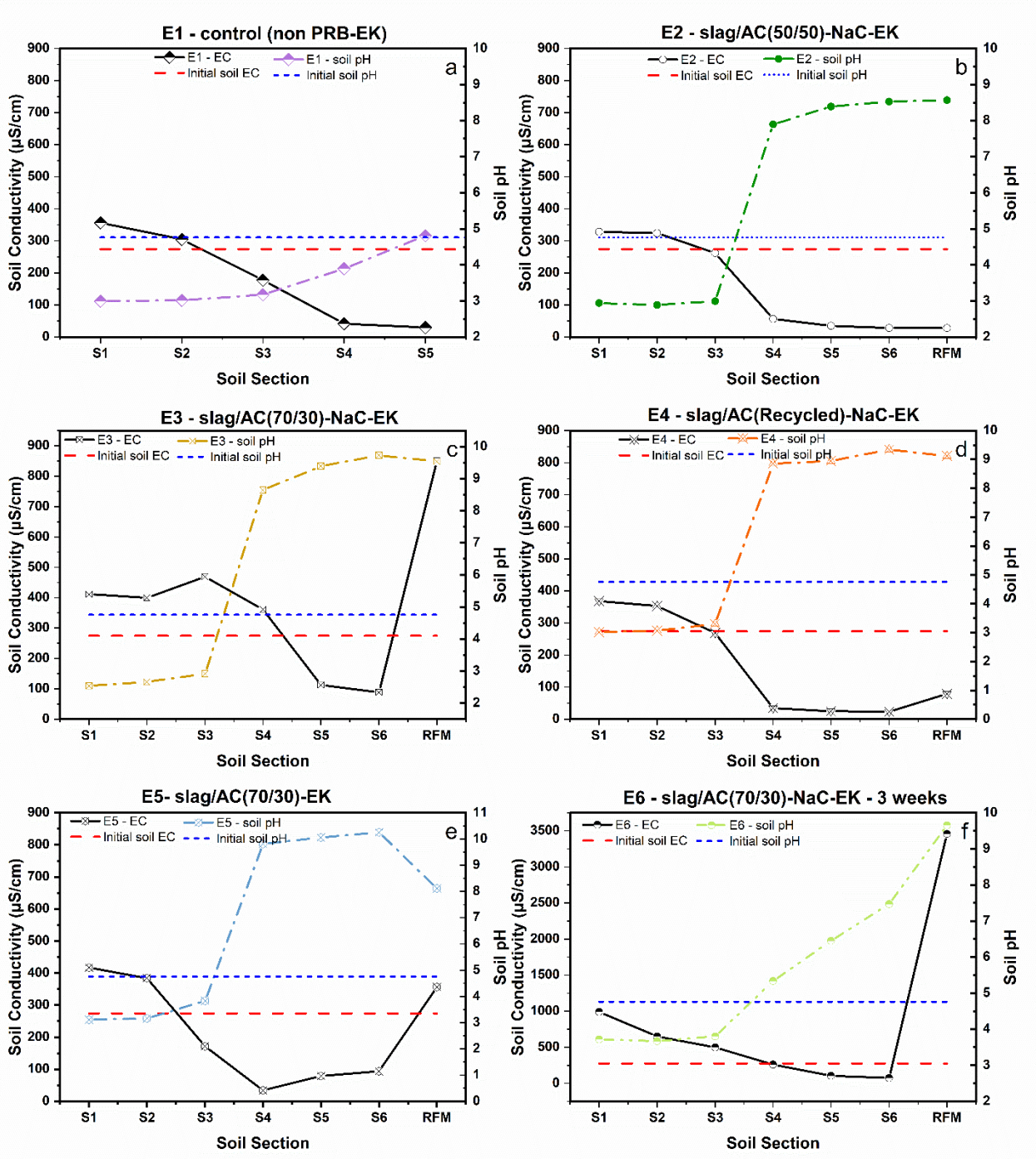

Figure 3: pH and EC of the soil after remediation in the sections from anode to cathode (a) experiment E1 (control) (b) experiment E2 (c) experiment E3 (d) experiment E4 (e) experiment E5 (f) experiment E6

3.3 Removal Rate

Figure 4a displays the residual concentration of perfluorooctanoic acid (PFOA) in each soil section and the permeable reactive barrier (PRB) after electrokinetic (EK) treatment. PFOA, characterized by a negatively charged nature and a hydrophilic functional group, can migrate within soil pore water under the influence of an electric field throughout the EK process. In experiment E1 (without PRB), a

notable observation can be made regarding the deposition of PFOA. A significant portion of the PFOA accumulated within the middle section. Due to the negative charge of PFOA, electromigration occurs in the anode direction, and electroosmosis occurs in the cathode direction. These mechanisms result in PFOA accumulation in the soil middle section. Previous experiments have also revealed PFOA deposition in the reactor's mid-area [21, 22, 48]. Consequently, the PRBs were utilized in the reactor cell's centre to enhance the efficacy of EK remediation in conjunction with NaC.

Figure 4a clearly demonstrates significant PFOA adsorption by the PRB and the migration of PFOA toward the anode region. Notably, the cathode region exhibits lower PFOA levels, which can be attributed to the increased pH resulting in decreased PFOA adsorption. The observed relationship between pH and PFOA adsorption supports the understanding that the sorption of PFOA is influenced by soil pH [45]. The charge of the soil is positive at pH values lower than the point of zero charge (pHzpc) and becomes negatively charged at pH values higher than the pHzpc. The adsorption of PFOA increases when the soil is positively charged near the anode region, as indicated by a pH value lower than the pHzpc (4.5). Conversely, PFOA adsorption on the soil decreases near the cathode region due to the high soil pH, with higher pH values than the pHzpc(4.5). Consequently, PFOA removal is more pronounced in the cathode zone due to two main factors: i) the electrostatic interaction between PFOA and the soil surface and ii) the electromigration of PFOA towards the anode. Another study reported a negative relationship between PFOA and pH, where an increase in pH led to decreased PFOA sorption in soil; the pH-PFOA adsorption relationship is consistent with earlier research [49].

The non-PRB EK test E1 removal rate was 33%, as shown in **Figure 4b**. However, when combined with PRB, the overall removal rate was doubled, with an E2 experimental result of 78%. E3 examined the effect of increasing the slag-to-AC ratio and found that the overall removal rate increase was not too significant, at 79%. When the PFOA adsorption onto PRB in E2 and E3 was compared, the experimental results were not significantly different (**Table 3**). When comparing the PFOA prevalence in soil sections, the residual PFOA concentration in soil sections S4-S6 in experiment E3 was negligible. In

addition, when the pH of two PRBs was compared, experiment E3 had a higher pH, which could be attributed to more slag. As a result, the residual PFOA concentration in soil sections after the EK process can be attributed to the slag content in the PRB. Experiment E4 evaluated the feasibility of recycled PRB in the EK process.

Additionally, the spent PRB was regenerated using methanol and subsequently reused in a subsequent cycle. The experimental findings demonstrate that the utilization of the spent PRB in the enhanced EK test resulted in a reduction of approximately 10% in the overall removal rate at 69%. The distribution of residual PFOA concentration in experiment E4 is illustrated in **Figure 4a**, where it can be observed that PFOA accumulated predominantly in sections S4 to S6 of the soil. This accumulation suggests that the PFOA migrated and deposited in these particular sections during the EK process. Experiment E4 PRB exhibited higher PFOA accumulation due to the reuse of spent material. In general, the reuse of PRB is feasible in the EK process, and the overall removal rate has remained relatively high.

To evaluate the importance of Sodium Cholate (NaC) in the PRB-enhanced EK process, experiment E5 was conducted without any surfactants. **Figure 4a** indicates the residual concentration of PFOA after the EK test E5; it can be seen that PFOA is distributed in the soil sections almost evenly, especially in S4-S6. NaC is an anionic surfactant facilitating PFOA transportation towards the anode due to lower critical micelle concentration (CMC). As a result, the absence of the biosurfactant resulted in a decrease in the overall removal rate (70.38%) in experiment E5, and PFOA accumulation was observed in soil sections S4-S5. Previous research conducted by our team has indicated that including sodium cholate (NaC) facilitated the transfer of PFOA toward the anode. Sodium cholate has a negative charge (-COO-), while PFOA carries a negative charge on the carboxylate functional group, forming a strong electrostatic interaction. Also, PFOA's non-polar part strongly interacts with the hydrophobic segment of NaC and transports toward the anode end. In addition to these interactions, hydrogen bonding can also play a role; both molecules possess hydrogen bonding capabilities. PFOA's functional group can form a hydrogen bond with NaC's hydroxyl group, leading to an additional attraction. Due to these

interactions, NaC enables PFOA's solubilization, mobilization and transport under an electric field in the EK process. Solubilization occurs by solubilizing PFOA by forming micelles. These micelles encapsulate the PFOA, effectively increasing their solubility in soil pore water and improving the contaminants' transportation by the EK process.

Furthermore, the results presented in **Figure 4** shed light on the effect of extending the experimental duration of the EK test to 3 weeks. The figure demonstrates a significant reduction in the residual concentration of PFOA in the soil sections compared to the 2-week experimental duration. This decrease in residual PFOA concentration signifies the successful adsorption of a substantial portion of PFOA onto the PRB employed in the EK system. **Figure 4a** depicts the experimental findings, showing that approximately 87% of the PFOA in the soil was effectively adsorbed onto the PRB, leading to an overall PFOA removal rate of 94% by the end of experiment E6 (**Table 3**). The residual concentration of PFOA in the soil was insignificant and primarily located near the anode region. This can be attributed to the acidic environment near the anode, which altered the surface charge of the soil and facilitated PFOA adsorption. In contrast, the soil section close to the cathode exhibited lower PFOA concentrations compared to the anode region due to the alkaline environment and the negative charge of the soil near the cathode, which hindered the adsorption of PFOA.

The observed reduction in PFOA concentration in the soil near the cathode and the substantial PFOA capture by the PRB highlight the crucial roles of electromigration and electroosmosis in transporting PFOA under the applied electric field. While the primary mechanism of PFOA adsorption onto the PRB is anticipated to be electrostatic interaction, it is important to note that some PFOA may also form inner sphere Fe-carboxylate complexes through ligand exchange, as reported in aqueous solutions [50]. In a related study, an electrochemical process was employed to degrade PFOA and PFOS, resulting in approximately 51.7% and 33% removal rates, respectively [48]. Our previous investigation focused on a surfactant-enhanced EK process, which successfully achieved around 75% PFOA removal with an initial concentration of 100 ppm [21]. Furthermore, a novel setup combining extraction with

462 stabilization in the EK system was explored, where a two-compartment configuration achieved 90%
463 PFOA removal, whilst a single-compartment setup reached a removal rate of 75% [20]. It is worth
464 noting that the duration of the EK process played a significant role in PFOA removal. Longer processing
465 times facilitated the transportation of PFOA and decreased its adsorption in the anode region,
466 suggesting that an extended experimental duration enhances the efficiency of PFOA removal in the
467 EK system.

468 Overall, incorporating iron slag/AC PRB in the EK improved PFOA removal, as demonstrated in
469 experiments E1 and E2. The affinity of iron slag to PFOA enhances its removal during the EK process.
470 Increasing the iron slag to AC ratio from 50%-50% in experiment E2 to 70%-30% in experiment E3
471 slightly increased the PFOA removal from 75% to 79.25%. Comparing experiments E3 and E5 shows
472 that PFOA removal was improved when NaC biosurfactant was dosed in the catholyte. PFOA removal
473 was 79.25% and 70.35% in experiments E3 and E5 (**Figure 4a**). Regenerated iron slag/AC PRB use in
474 the EK process decreased the PFOA removal from 79.25% in experiment E3 to 63.92% in experiment
475 E4. The maximum PFOA removal was 94% in experiment E6 due to the longer process duration.

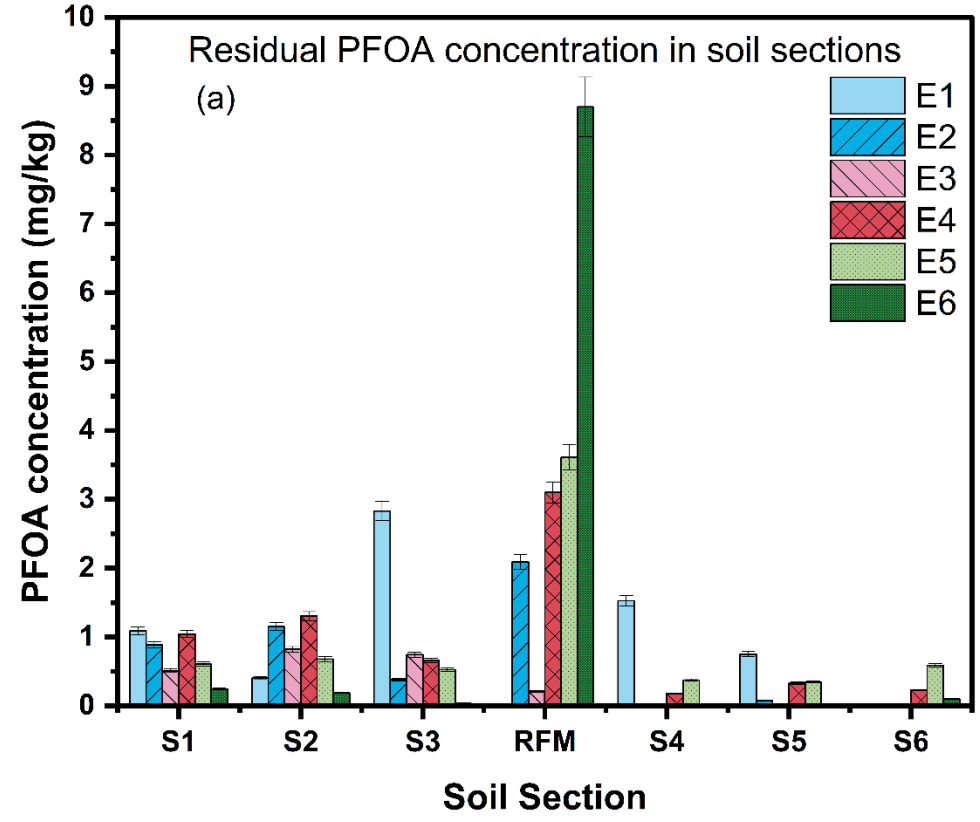

476

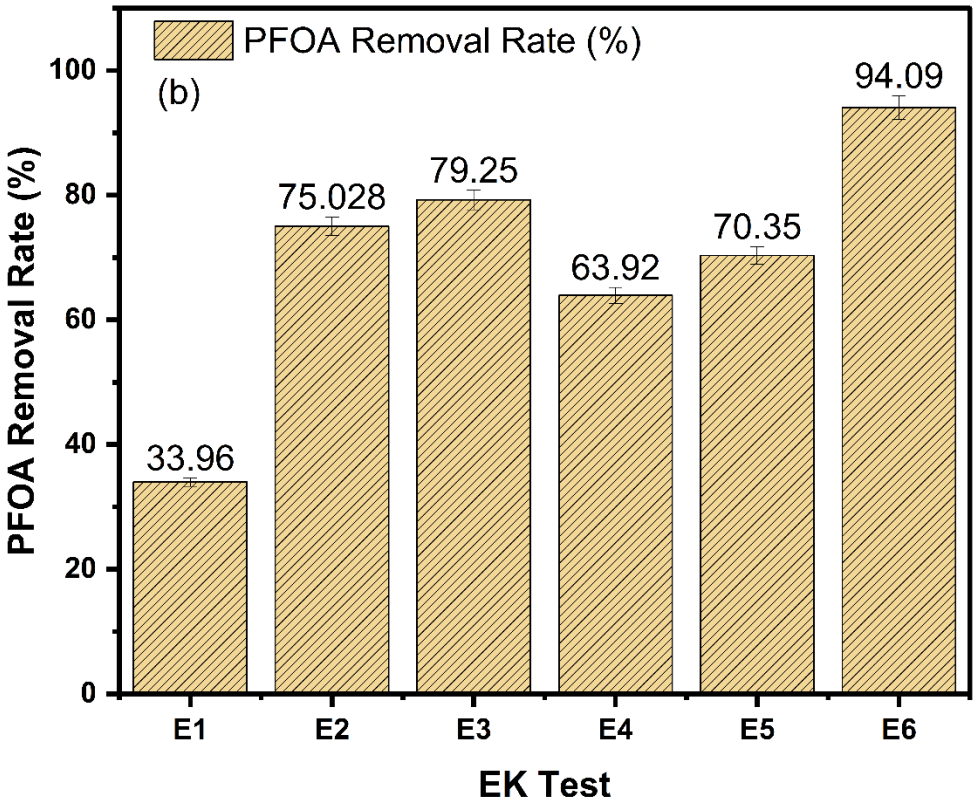

477

478 **Figure 4: (a) Residual PFOA concentration in soil sections post EK treatment (b) PFOA removal at the end of the EK**
479 **process.**

480 **Table 3: Mass Balance and Removal efficiency of EK tests**

Experiments	Initial PFOA in soil (mg)	Residual PFOA in treated soil (mg)	PFOA mass in PRB (mg)	PFOA mass in the electrolyte (mg)	Mass balance (%)	PFOA removal (%)
E1	10	6.8911	-	3.0725	99.65	33.16±0.11
E2	10	2.3806	2.0901	5.5293	98.04	78.93±0.09
E3	10	2.0749	2.1188	5.9576	101.12	79.25±0.15
E4	10	3.7491	3.1475	3.6199	101.21	69.91±0.12
E5	10	3.1223	3.6112	3.0888	98.36	70.38±0.09
E6	10	0.5904	8.7124	1.6004	109.07	94.09±0.16

481

482 ***3.4 Characteristics of PRB***

483 **Figure 5a** exhibits the XRD result of the steel-making iron slag components. The results indicate that
484 the main component of the slag is iron oxide, and iron oxide has an adsorption capacity to remove
485 contaminations [37]. PFOA's primary adsorption mechanism is electrostatic interaction, and PFOA
486 forms inner sphere Fe-carboxylate complexes by ligand exchange [51]. pHzpc is the pH at which the
487 net surface charge is zero. It determines the adsorbent's interaction with electrolytes and influences
488 the ion exchange capacity [52]. The pHzpc was measured for the PRB used in the EK experiment to
489 evaluate the PRB and PFOA adsorption mechanism, and the pHzpc of the PRB used was 9.5. Basic
490 oxides possess a positive surface charge around pzc 9.4-9 [53]. Because the surface charge of the PRB
491 is positive and PFOA is anionic, the adsorption mechanism onto the PRB is most likely an electrostatic
492 interaction.

493 Steel slag, a solid waste material, possesses favorable characteristics such as a high specific surface
494 area and large porosity. It is a potential low-cost adsorbent for removing contaminants from water
495 and soil [54]. The capacity and efficiency of steel slag for pollutant removal are influenced by its
496 surface physiochemical characteristics and chemical components. In the context of removing PFOA
497 from contaminated water and soil, activated carbon has conventionally been employed as the
498 adsorbent [55, 56]. Accordingly, our study used a mixture of activated carbon and slag as the
499 permeable reactive barrier (PRB) to adsorb PFOA in the electrokinetic (EK) process. The components
500 of the slag were analyzed using an X-ray diffraction (XRD) analyzer, as shown in **Figure 5a.** The

interaction between iron oxide and PFOA is not yet fully understood; however, iron oxide can undergo adsorption or surface attachment reactions with PFOA in the environment. Due to its small particle size and high porosity, iron oxide exhibits a substantial surface area, rendering it an excellent adsorbent [57]. The primary mechanism for the adsorption of PFOA onto iron oxide involves electrostatic interactions between PFOA molecules, with subsequent formation of inner-sphere Fe-carboxylate complexes through ligand exchange [50]. The adsorption of PFOA onto iron oxide particles can have several implications. Firstly, it can reduce the mobility of PFOA in the environment, thereby decreasing the likelihood of contaminating groundwater or leaching into the surrounding areas. Furthermore, the adsorption of PFOA onto iron oxide particles can affect the particle's behaviour and properties, such as stability and reactivity [58].

The Fourier-transform infrared spectroscopy (FTIR) results provide valuable insights into the functional groups present in the sample. As shown in **Figure 5b, a strong band observed in the 1100-1000 cm-1 range** corresponds to the C-O stretching vibrations. Additionally, a broad band around 3400-3200 cm^{-1} indicates the presence of O-H stretching vibrations. The band observed in the 1700-1600 cm-1 range corresponds to the C=O stretching vibrations of carboxylic acid. Another band observed in the 1600-1450 cm-1 range corresponds to the C=C stretching vibrations. These functional group vibrations are characteristic of activated carbon, as evidenced by the initial PRB FTIR spectrum. However, after conducting the electrokinetic (EK) experiments, these vibrations became more prominent, indicating the adsorption of PFOA in the PRB. In particular, a band around 1250-1180 cm^{-1} corresponds to the C-F stretching vibrations of the fluorinated carbon chain, while a band around 1000 cm^{-1} corresponds to the stretching vibrations of the ether group (-O-CF2-). These bands confirm the presence of PFOA adsorbed by the PRB. The intensity and strength of these bands are higher in regions where the adsorption of PFOA is more pronounced. Furthermore, the analysis of adsorption kinetics revealed that both physical adsorption and chemical adsorption mechanisms contribute to the adsorption of PFOA onto PRB, where pseudo-second-order kinetics fitted well (R^2: 0.99 for PRB) (**Figure 5c).**

BET of the PRB before and after the EK process was analyzed using the density functional theory (DFT) because, according to the literature, it has higher accuracy than Barrett-Joyner-Halenda (BJH) theory [59]. The experimental findings revealed variations in the specific surface area of PRB before and after the EK tests. Prior to the EK test, the PRB exhibited a specific surface area of 243.06 m^2/g. However, after experiment E2, the specific surface area decreased to 40.73 m^2/g. In contrast, experiment E6, which spanned 3 weeks, further reduced the specific surface area to 18.927 m^2/g. This decrease can be attributed to the accumulation of high levels of PFOA on the surface of the PRB following the EK test. It is noteworthy that the regenerated PRB, after the EK test, exhibited a BET result indicating a specific surface area of 52.459 m^2/g. The slight increase in the BET of regenerated and reused PRB can be attributed to modifying the PRB surface during the recycling and EK treatment process.

The energy-dispersive X-ray spectroscopy (EDS) results of the PRB utilized in the EK tests are presented in **Figures 5d** to **5g**. **Figure 5d** displays the EDS image of the PRB before undergoing EK treatment. **Figure 5e** exhibits the image of the PRB after 2 weeks of EK treatment, while **Figure 5f (experiment E4)** represents the EDS image of the recycled PRB following 2 weeks of the EK process. **Figure 5g** illustrates the PRB after the 3-week EK experiment (experiment E6). Analyzing the EDS figures reveals variations in the iron content, particularly in experiment E6 (**Figure 5g**). This lower iron content can be attributed to the highest adsorption of PFOA onto the PRB, covering the iron surface. PRB analysis showed that 8.7 mg PFOA was adsorbed onto the iron slag PRB in experiment E6 compared to 2.118 g and 3.147 g in experiments E3 and E4 (Table 3). The higher PFOA adsorption in experiment E6 explains the EDS results in Figures 5e, 5f, and 5g. Compared to Figures 5e to 5g, the lower iron in Figure 5d could be due to more AC in the iron slag/AC sample. The EDS results provide visual evidence of the changes in elemental composition resulting from the interaction between the PRB and the PFOA during the EK process.

550

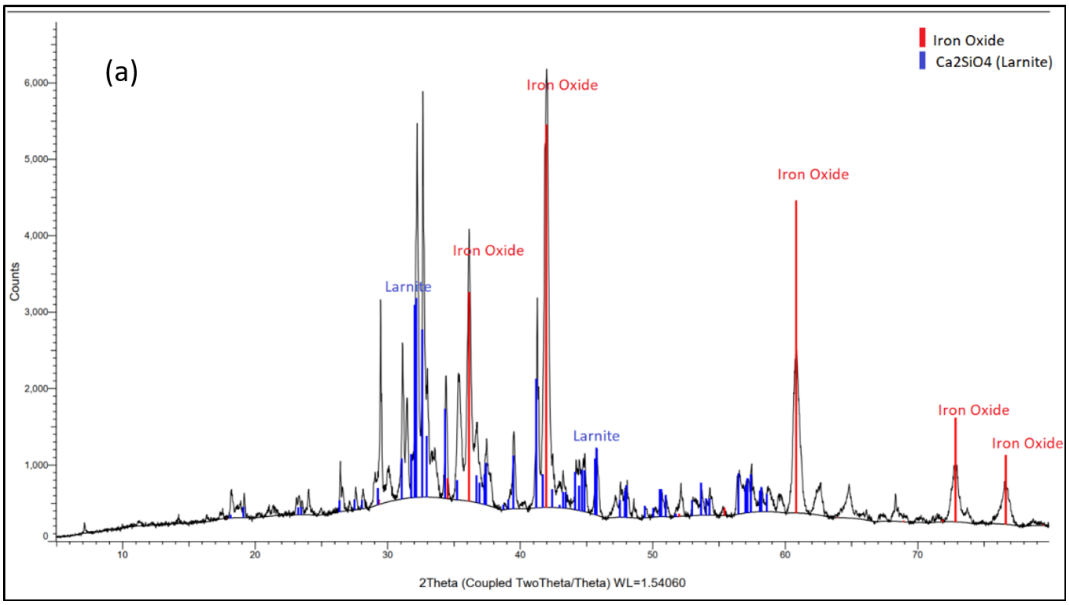
(a)
Iron Oxide
Ca2SiO4 (Larnite)
Iron Oxide
Iron Oxide
Iron Oxide
Larnite
Larnite
Iron Oxide
Iron Oxide
Counts
2Theta (Coupled TwoTheta/Theta) WL=1.54060

551

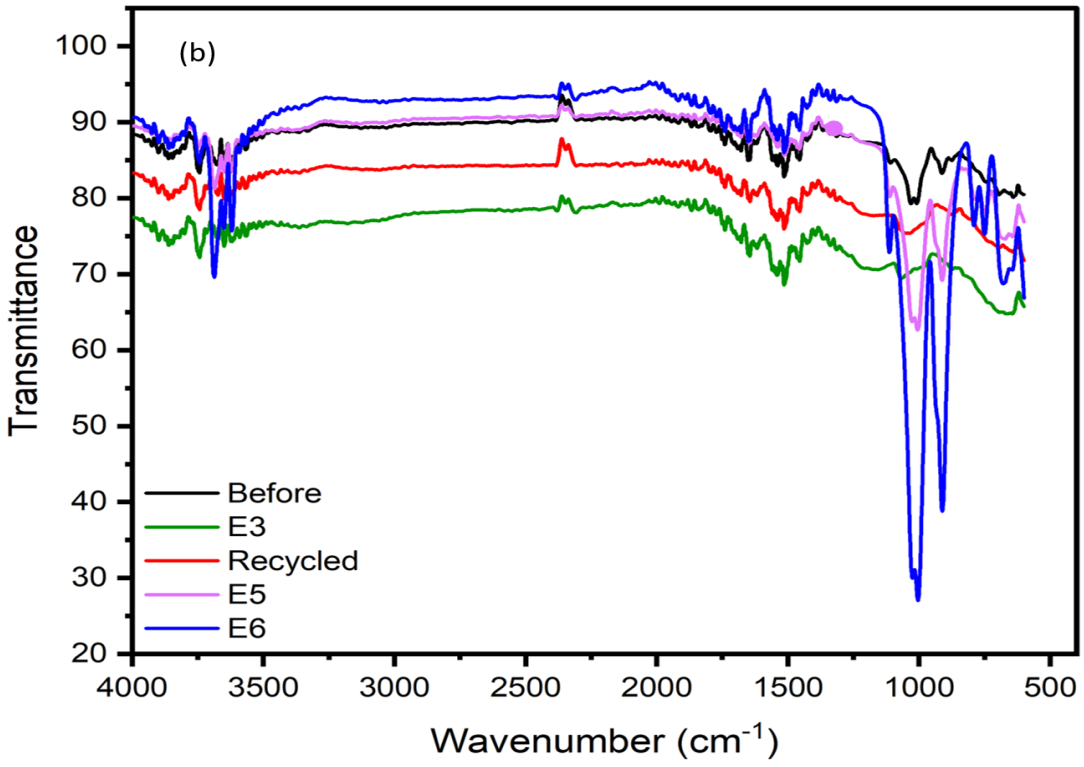
(b)
Transmittance
Wavenumber (cm-1)
Before
E3
Recycled
E5
E6

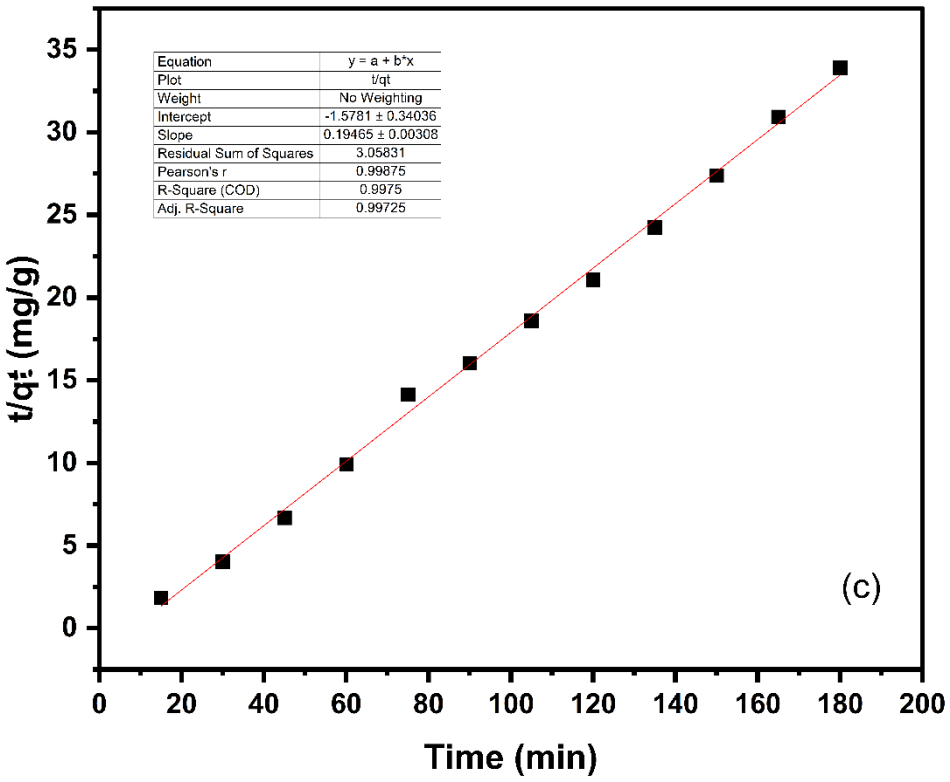
Equation y = a + b*x
Plot t/qt
Weight No Weighting
Intercept -1.5781 ± 0.34036
Slope 0.19465 ± 0.00308
Residual Sum of Squares 3.05831
Pearson's r 0.99875
R-Square (COD) 0.9975
Adj. R-Square 0.99725
t/qt (mg/g)
Time (min)
(c)

552

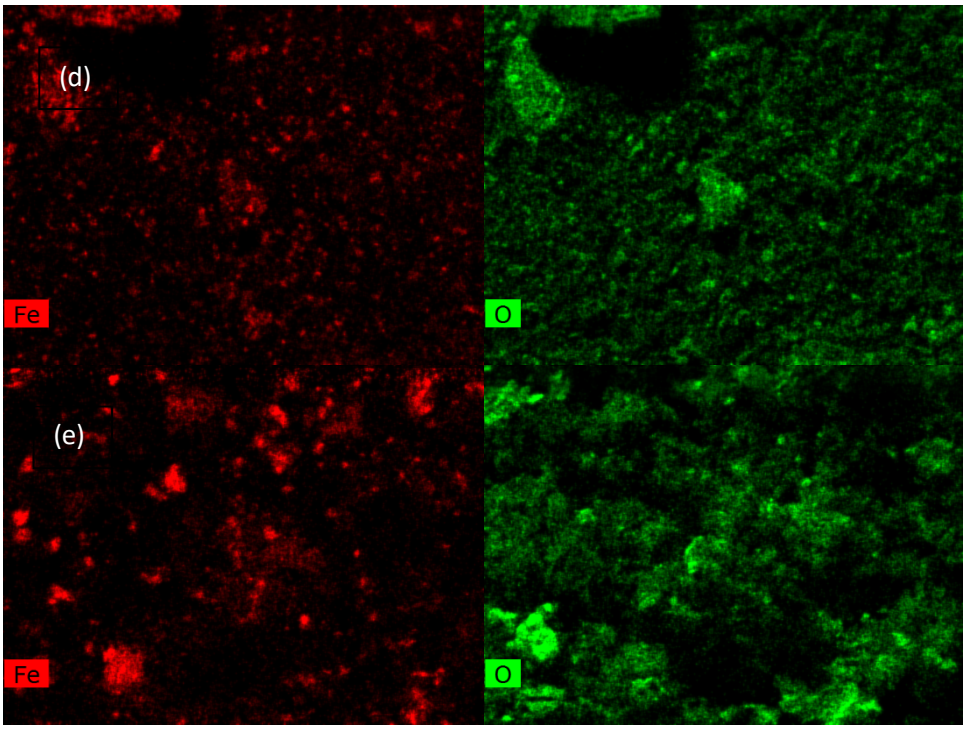
(d)
Fe
O
(e)
Fe
O

553

554

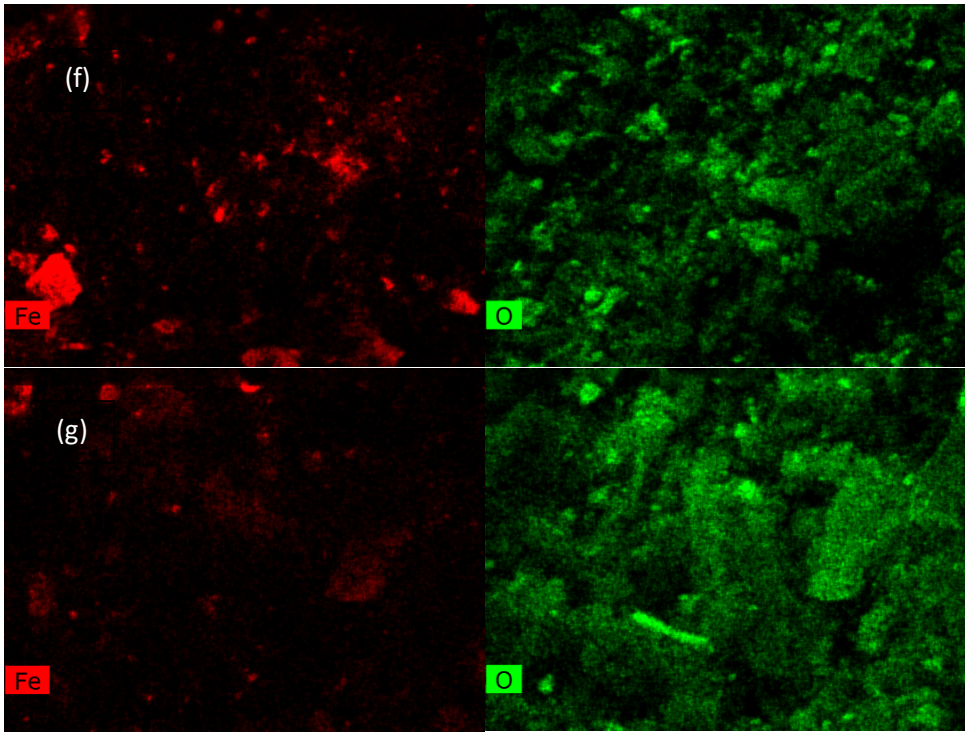

555

556

557 **Figure 5: (a) Slag XRD spectrum (b) FTIR results of PRB before and after EK tests (c) Pseudo Second-order kinetic**
558 **model (d) EDS results of PRB before EK tests (e) EDS results of PRB after EK test (E3) (f) EDS of PRB after E4**
559 **(recycled PRB) (g) EDS of PRB after E6**

560

561 ***3.5 Specific Energy Consumption***

562 Calculating specific energy consumption is important in determining overall energy consumption and

563 treatment costs. The following equation calculated the SEC for all experiments:

564 $$E_u = \frac{1}{V_s} \int V\, I\, dt \qquad \text{(Equation 2)}$$

565 Where V_s is the total soil volume (kg), V is the average applied voltage (V), I is electric current (A),
566 and t is the treatment time (h).

567 **Figure 6** depicts the SEC in comparison with the overall removal rate. As can be seen, there is no direct

568 relationship between the removal rate and energy consumption. However, the higher the average

569 current of the EK test, the higher the SEC. Hence it is related to the energy it took to push the

570 contaminants under an electric field. Experiment E3 had higher SEC (0.1059 kWh/kg) than E2 (0.0704

571 kWh/kg) due to having a higher average electric current, 10.51 mA and 13.39 mA, respectively. This

572 result can be attributed to the slag content in the PRB. Higher slag content was more conducive.

573 However, recycled slag PRB exhibited higher SEC (0.1214 kWh/kg), which was due to a higher average

electric current (19.74 mA) which was similar to experiment E5 (19.27 mA) with SEC (0.1178 kWh/kg). The average higher current can be attributed to the lower average voltage and taking more energy to push through the contaminants across the soil medium. Increasing processing time has also increased the average current attributed to the higher SEC (0.1517 kWh/kg). However, considering the overall removal rate of 94.09% in experiment E6, the SEC is not significantly higher. The EK electroosmotic flow did not exhibit a direct correlation with the overall removal rate and the specific energy consumption of the EK process, as illustrated in Figure 6. Compared to PRB-enhanced EK tests E2 to E6, experiment E1 exhibited the lower electroosmotic flow due to low electric current (Figure 2a).

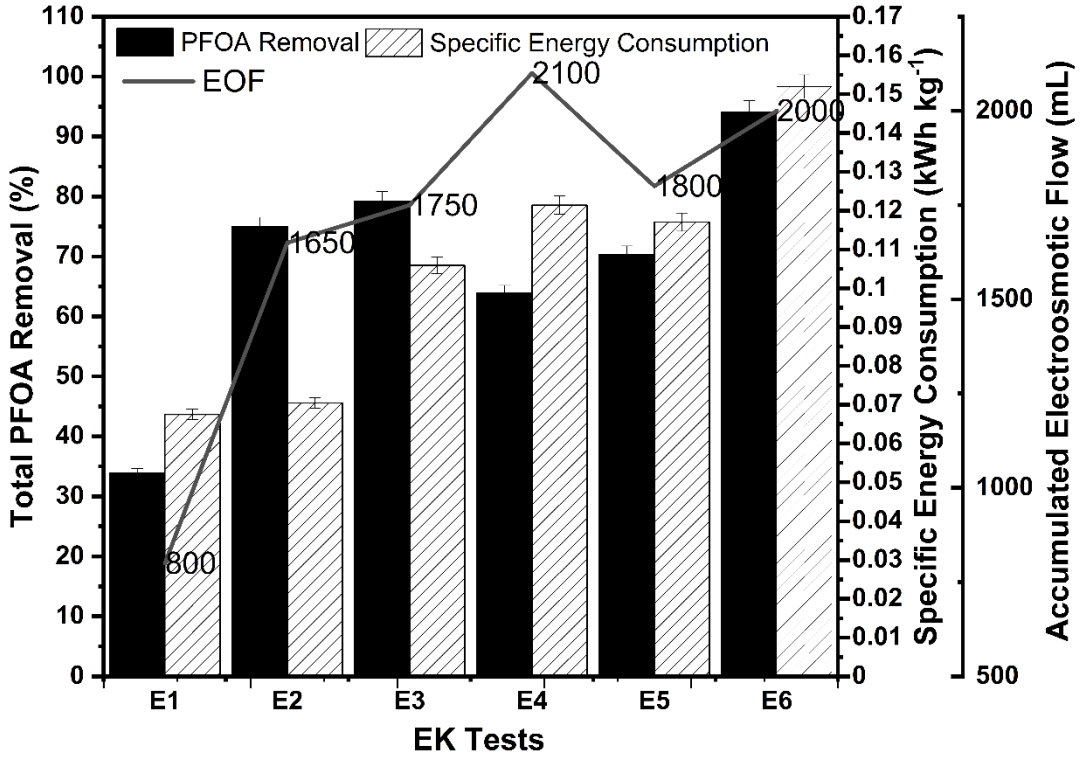

Figure 6: Specific Energy Consumption (SEC), accumulated electroosmotic flow (EOF) of all EK tests and the overall removal rate

Conclusion

This work confirms the applicability of iron slag/AC mixture as PRB in the EK process for PFOA treatment. The iron slag/AC PRB is inexpensive, available, has an excellent PFOA adsorption capacity and can be easily incorporated into the EK reactor. In the Ek process, PFOA was captured by the PRB and was easily recovered by a suitable solvent. Reusing slag in the EK process to capture PFOA from contaminated soil is an environmentally sustainable method with a promising future. Slag is typically disposed of in landfills because it is industrial waste. Slag/AC PRB enhanced EK test in conjunction with sodium cholate biosurfactant is an environmentally friendly method for PFOA removal. EK tests with 70/30 iron slag to AC PRB achieved the best PFOA removal from the kaolinite soil. After two weeks of treatment with 20mA constant current, the overall removal rate was 79%, with approximately 20% adsorbed onto PRB and the majority pushed into the catholyte overflow. However, when the experiment was extended to three weeks, the overall removal rate rose to 95%, and nearly 87% of PFOA was adsorbed onto PRB. The adsorbed PFOA was easily recovered from the PRB by methanol. The importance of biosurfactant was also assessed, and the results show that it plays an important role in the transport of PFOA towards the anode region or the PRB to be captured.

Generally, the iron slag/AC-enhanced EK process can potentially remove PFOA from real contaminated sites. The slag/AC PRB has strong adsorption to FPOA and can be extracted at the end of the EK process for PFOA extraction. The latter process will be quick due to the high iron slag permeability (Table 1).

Acknowledgement:

This publication was made possible by MME grant MME01-0906- 190024 from the Qatar National Research Fund (a member of Qatar Foundation). The findings achieved herein are solely the author's responsibility.

Reference

[1] E. Barth, J. McKernan, D. Bless, K. Dasu, Investigation of an immobilization process for PFAS contaminated soils, Journal of Environmental Management, 296 (2021) 113069-113069.
[2] C.E. Schaefer, C. Andaya, A. Urtiaga, E.R. McKenzie, C.P. Higgins, Electrochemical treatment of perfluorooctanoic acid (PFOA) and perfluorooctane sulfonic acid (PFOS) in groundwater impacted by aqueous film forming foams (AFFFs), Journal of Hazardous Materials, 295 (2015) 170-175.
[3] M.L. Brusseau, R.H. Anderson, B. Guo, PFAS concentrations in soils: Background levels versus contaminated sites, Science of The Total Environment, 740 (2020) 140017-140017.
[4] M.B. Ahmed, M.A.H. Johir, R. McLaughlan, L.N. Nguyen, B. Xu, L.D. Nghiem, Per- and polyfluoroalkyl substances in soil and sediments: Occurrence, fate, remediation and future outlook, Science of the Total Environment, 748 (2020) 141251-141251.
[5] N. Bolan, B. Sarkar, Y. Yan, Q. Li, H. Wijesekara, K. Kannan, D.C.W. Tsang, M. Schauerte, J. Bosch, H. Noll, Y.S. Ok, K. Scheckel, J. Kumpiene, K. Gobindlal, M. Kah, J. Sperry, M.B. Kirkham, H. Wang, Y.F. Tsang, D. Hou, J. Rinklebe, Remediation of poly- and perfluoroalkyl substances (PFAS) contaminated soils – To mobilize or to immobilize or to degrade?, Journal of Hazardous Materials, 401 (2021) 123892-123892.
[6] T.L. Coggan, D. Moodie, A. Kolobaric, D. Szabo, J. Shimeta, N.D. Crosbie, E. Lee, M. Fernandes, B.O. Clarke, An investigation into per- and polyfluoroalkyl substances (PFAS) in nineteen Australian wastewater treatment plants (WWTPs), Heliyon, 5 (2019) e02316-e02316.
[7] N.Z. Epa Au, PFAS National Environmental Management Plan VERSION 2.0 CONSULTATION DRAFT, 2019.
[8] D. Longpré, L. Lorusso, C. Levicki, R. Carrier, P. Cureton, PFOS, PFOA, LC-PFCAS, and certain other PFAS: A focus on Canadian guidelines and guidance for contaminated sites management, Environmental Technology and Innovation, 18 (2020) 100752-100752.
[9] R. Mahinroosta, L. Senevirathna, A review of the emerging treatment technologies for PFAS contaminated soils, Journal of Environmental Management, 255 (2020) 109896-109896.
[10] M.W. Sima, P.R. Jaffé, A critical review of modeling Poly- and Perfluoroalkyl Substances (PFAS) in the soil-water environment, Science of the Total Environment, 757 (2021) 143793-143793.
[11] S.E. Hale, H.P.H. Arp, G.A. Slinde, E.J. Wade, K. Bjørseth, G.D. Breedveld, B.F. Straith, K.G. Moe, M. Jartun, Å. Høisæter, Sorbent amendment as a remediation strategy to reduce PFAS mobility and leaching in a contaminated sandy soil from a Norwegian firefighting training facility, Chemosphere, 171 (2017) 9-18.
[12] M. Askeland, B.O. Clarke, S.A. Cheema, A. Mendez, G. Gasco, J. Paz-Ferreiro, Biochar sorption of PFOS, PFOA, PFHxS and PFHxA in two soils with contrasting texture, Chemosphere, 249 (2020) 126072-126072.
[13] M. Sörengård, P. Gago-Ferrero, D. B. Kleja, L. Ahrens, Laboratory-scale and pilot-scale stabilization and solidification (S/S) remediation of soil contaminated with per- and polyfluoroalkyl substances (PFASs), Journal of Hazardous Materials, 402 (2021) 123453-123453.
[14] M. Sörengård, A.S. Lindh, L. Ahrens, Thermal desorption as a high removal remediation technique for soils contaminated with per- and polyfluoroalkyl substances (PFASs), PloS one, 15 (2020) e0234476-e0234476.
[15] L.P. Turner, B.H. Kueper, K.M. Jaansalu, D.J. Patch, N. Battye, O. El-Sharnouby, K.G. Mumford, K.P. Weber, Mechanochemical remediation of perfluorooctanesulfonic acid (PFOS) and perfluorooctanoic acid (PFOA) amended sand and aqueous film-forming foam (AFFF) impacted soil by planetary ball milling, Science of the Total Environment, 765 (2021) 142722-142722.
[16] C. Grimison, E.R. Knight, T.M.H. Nguyen, N. Nagle, S. Kabiri, J. Bräunig, D.A. Navarro, R.S. Kookana, C.P. Higgins, M.J. McLaughlin, J.F. Mueller, The efficacy of soil washing for the remediation of per- and poly-fluoroalkyl substances (PFASs) in the field, Journal of Hazardous Materials, 445 (2023) 130441.
[17] Å. Høisæter, H.P.H. Arp, G. Slinde, H. Knutsen, S.E. Hale, G.D. Breedveld, M.C. Hansen, Excavated vs novel in situ soil washing as a remediation strategy for sandy soils impacted with per-

659 and polyfluoroalkyl substances from aqueous film forming foams, Science of The Total Environment,
660 794 (2021) 148763.
661 [18] R. Kumar, T.K. Dada, A. Whelan, P. Cannon, M. Sheehan, L. Reeves, E. Antunes, Microbial and
662 thermal treatment techniques for degradation of PFAS in biosolids: A focus on degradation
663 mechanisms and pathways, Journal of Hazardous Materials, 452 (2023) 131212.
664 [19] E. Shahsavari, D. Rouch, L.S. Khudur, D. Thomas, A. Aburto-Medina, A.S. Ball, Challenges and
665 Current Status of the Biological Treatment of PFAS-Contaminated Soils, Frontiers in Bioengineering
666 and Biotechnology, 8 (2021) 1-15.
667 [20] G. Niarchos, M. Sörengård, F. Fagerlund, L. Ahrens, Electrokinetic remediation for removal of
668 per- and polyfluoroalkyl substances (PFASs) from contaminated soil, Chemosphere, 291 (2022)
669 133041.
670 [21] N. Ganbat, A. Altaee, J.L. Zhou, T. Lockwood, R.A. Al-Juboori, F.M. Hamdi, E. Karbassiyazdi, A.K.
671 Samal, A. Hawari, H. Khabbaz, Investigation of the effect of surfactant on the electrokinetic
672 treatment of PFOA contaminated soil, Environmental Technology & Innovation, (2022) 102938.
673 [22] M. Sörengård, G. Niarchos, P.E. Jensen, L. Ahrens, Electrodialytic per- and polyfluoroalkyl
674 substances (PFASs) removal mechanism for contaminated soil, Chemosphere, 232 (2019) 224-231.
675 [23] Y.B. Acar, A.N. Alshawabkeh, Principles of electrokinetic remediation, Environmental Science &
676 Technology, 27 (1993) 2638-2647.
677 [24] M.T. Alcántara, J. Gómez, M. Pazos, M.A. Sanromán, Electrokinetic remediation of PAH mixtures
678 from kaolin, Journal of Hazardous Materials, 179 (2010) 1156-1160.
679 [25] A. Colacicco, G. De Gioannis, A. Muntoni, E. Pettinao, A. Polettini, R. Pomi, Enhanced
680 electrokinetic treatment of marine sediments contaminated by heavy metals and PAHs,
681 Chemosphere, 81 (2010) 46-56.
682 [26] R. Ghobadi, A. Altaee, J.L. Zhou, E. Karbassiyazdi, N. Ganbat, Effective remediation of heavy
683 metals in contaminated soil by electrokinetic technology incorporating reactive filter media, Science
684 of the Total Environment, 794 (2021) 148668-148668.
685 [27] D.C. Andrade, E.V. dos Santos, Combination of electrokinetic remediation with permeable
686 reactive barriers to remove organic compounds from soils, Current Opinion in Electrochemistry, 22
687 (2020) 136-144.
688 [28] Y. Sun, K. Gao, Y. Zhang, H. Zou, Remediation of persistent organic pollutant-contaminated soil
689 using biosurfactant-enhanced electrokinetics coupled with a zero-valent iron/activated carbon
690 permeable reactive barrier, Environmental Science and Pollution Research, 24 (2017) 28142-28151.
691 [29] J.-G. Han, K.-K. Hong, Y.-W. Kim, J.-Y. Lee, Enhanced electrokinetic (E/K) remediation on copper
692 contaminated soil by CFW (carbonized foods waste), Journal of Hazardous Materials, 177 (2010)
693 530-538.
694 [30] R. Ghobadi, A. Altaee, J.L. Zhou, P. McLean, N. Ganbat, D. Li, Enhanced copper removal from
695 contaminated kaolinite soil by electrokinetic process using compost reactive filter media, Journal of
696 Hazardous Materials, 402 (2020) 123891-123891.
697 [31] C. Cameselle, K.R. Reddy, Development and enhancement of electroosmotic flow for the
698 removal of contaminants from soils, Electrochimica Acta, 86 (2012) 10-22.
699 [32] Z. Li, S. Yuan, J. Wan, H. Long, M. Tong, A combination of electrokinetics and Pd/Fe PRB for the
700 remediation of pentachlorophenol-contaminated soil, Journal of Contaminant Hydrology, 124 (2011)
701 99-107.
702 [33] D. Ren, S. Li, J. Wu, L. Fu, X. Zhang, S. Zhang, Remediation of Phenanthrene-Contaminated Soil
703 by Electrokinetics Coupled with Iron/Carbon Permeable Reactive Barrier, Environmental Engineering
704 Science, 36 (2019) 1224-1235.
705 [34] H. Zhou, J. Xu, S. Lv, Z. Liu, W. Liu, Removal of cadmium in contaminated kaolin by new-style
706 electrokinetic remediation using array electrodes coupled with permeable reactive barrier,
707 Separation and Purification Technology, 239 (2020) 116544-116544.

[35] E. Vieira dos Santos, C. Sáez, P. Cañizares, C.A. Martínez-Huitle, M.A. Rodrigo, Reversible electrokinetic adsorption barriers for the removal of atrazine and oxyfluorfen from spiked soils, Journal of Hazardous Materials, 322 (2017) 413-420.
[36] X. Wang, X. Li, X. Yan, C. Tu, Z. Yu, Environmental risks for application of iron and steel slags in soils in China: A review, Pedosphere, 31 (2021) 28-42.
[37] M. Díaz-Piloneta, F. Ortega-Fernández, M. Terrados-Cristos, J.V. Álvarez-Cabal, Application of Steel Slag for Degraded Land Remediation, in: Land, 2022.
[38] J. Zhan, A. Zhang, P. Héroux, Y. Guo, Z. Sun, Z. Li, J. Zhao, Y. Liu, Remediation of perfluorooctanoic acid (PFOA) polluted soil using pulsed corona discharge plasma, Journal of Hazardous Materials, 387 (2020) 121688-121688.
[39] C. CARE, Assessment, management and remediation for PFOS and PFOA Part 1: background, in: Technical Report No. 38. CRC for Contamination Assessment and Remediation of the Environment, Australia Newcastle, 2017.
[40] A. Altaee, R. Smith, S. Mikhalovsky, The feasibility of decontamination of reduced saline sediments from copper using the electrokinetic process, Journal of Environmental Management, 88 (2008) 1611-1618.
[41] J. Zhan, A. Zhang, P. Héroux, Y. Guo, Z. Sun, Z. Li, J. Zhao, Y. Liu, Remediation of perfluorooctanoic acid (PFOA) polluted soil using pulsed corona discharge plasma, Journal of Hazardous Materials, 387 (2020) 121688.
[42] P. Guedes, V. Lopes, N. Couto, E.P. Mateus, C.S. Pereira, A.B. Ribeiro, Electrokinetic remediation of contaminants of emergent concern in clay soil: Effect of operating parameters, Environmental Pollution, 253 (2019) 625-635.
[43] J. Wan, Z. Li, X. Lu, S. Yuan, Remediation of a hexachlorobenzene-contaminated soil by surfactant-enhanced electrokinetics coupled with microscale Pd/Fe PRB, Journal of Hazardous Materials, 184 (2010) 184-190.
[44] M. Millán, P.Y. Bucio-Rodríguez, J. Lobato, C.M. Fernández-Marchante, G. Roa-Morales, C. Barrera-Díaz, M.A. Rodrigo, Strategies for powering electrokinetic soil remediation: A way to optimize performance of the environmental technology, Journal of environmental management, 267 (2020) 110665-110665.
[45] F. Wang, K. Shih, Adsorption of perfluorooctanesulfonate (PFOS) and perfluorooctanoate (PFOA) on alumina: influence of solution pH and cations, Water Res, 45 (2011) 2925-2930.
[46] D.P. Oliver, Y. Li, R. Orr, P. Nelson, M. Barnes, M.J. McLaughlin, R.S. Kookana, The role of surface charge and pH changes in tropical soils on sorption behaviour of per- and polyfluoroalkyl substances (PFASs), Science of The Total Environment, 673 (2019) 197-206.
[47] R.L. Johnson, A.J. Anschutz, J.M. Smolen, M.F. Simcik, R.L. Penn, The Adsorption of Perfluorooctane Sulfonate onto Sand, Clay, and Iron Oxide Surfaces, Journal of Chemical & Engineering Data, 52 (2007) 1165-1170.
[48] J. Hou, G. Li, M. Liu, L. Chen, Y. Yao, P.H. Fallgren, S. Jin, Electrochemical destruction and mobilization of perfluorooctanoic acid (PFOA) and perfluorooctane sulfonate (PFOS) in saturated soil, Chemosphere, 287 (2022) 132205-132205.
[49] T. Groffen, J. Rijnders, N. Verbrigghe, E. Verbruggen, E. Prinsen, M. Eens, L. Bervoets, Influence of soil physicochemical properties on the depth profiles of perfluoroalkylated acids (PFAAs) in soil along a distance gradient from a fluorochemical plant and associations with soil microbial parameters, Chemosphere, 236 (2019) 124407-124407.
[50] X. Gao, J. Chorover, Adsorption of perfluorooctanoic acid and perfluorooctanesulfonic acid to iron oxide surfaces as studied by flow-through ATR-FTIR spectroscopy, Environmental Chemistry, 9 (2012) 148-157.
[51] S.-K. Ahn, K.-Y. Park, W.-j. Song, Y.-m. Park, J.-H. Kweon, Adsorption mechanisms on perfluorooctanoic acid by FeCl3 modified granular activated carbon in aqueous solutions, Chemosphere, 303 (2022) 134965.

[52] H.R. Pouretedal, N. Sadegh, Effective removal of Amoxicillin, Cephalexin, Tetracycline and Penicillin G from aqueous solutions using activated carbon nanoparticles prepared from vine wood, Journal of Water Process Engineering, 1 (2014) 64-73.
[53] P. Tengvall, 4.6 Protein Interactions With Biomaterials☆, in: P. Ducheyne (Ed.) Comprehensive Biomaterials II, Elsevier, Oxford, 2017, pp. 70-84.
[54] C. Shi, X. Wang, S. Zhou, X. Zuo, C. Wang, Mechanism, application, influencing factors and environmental benefit assessment of steel slag in removing pollutants from water: A review, Journal of Water Process Engineering, 47 (2022) 102666.
[55] S. Deng, Y. Nie, Z. Du, Q. Huang, P. Meng, B. Wang, J. Huang, G. Yu, Enhanced adsorption of perfluorooctane sulfonate and perfluorooctanoate by bamboo-derived granular activated carbon, Journal of Hazardous Materials, 282 (2015) 150-157.
[56] Y.C. Lee, Y.f. Li, M.J. Chen, Y.C. Chen, J. Kuo, S.L. Lo, Efficient decomposition of perfluorooctanic acid by persulfate with iron-modified activated carbon, Water Research, 174 (2020).
[57] M. Jain, M. Yadav, T. Kohout, M. Lahtinen, V.K. Garg, M. Sillanpää, Development of iron oxide/activated carbon nanoparticle composite for the removal of Cr(VI), Cu(II) and Cd(II) ions from aqueous solution, Water Resources and Industry, 20 (2018) 54-74.
[58] M. Hassan, Y. Liu, R. Naidu, J. Du, F. Qi, Adsorption of Perfluorooctane sulfonate (PFOS) onto metal oxides modified biochar, Environmental Technology and Innovation, 19 (2020) 100816-100816.
[59] R. Bardestani, G.S. Patience, S. Kaliaguine, Experimental methods in chemical engineering: specific surface area and pore size distribution measurements—BET, BJH, and DFT, The Canadian Journal of Chemical Engineering, 97 (2019) 2781-2791.